Research Article

Control and Impact of Metal Loading Heterogeneities at the Nanoscale on the Performance of Pt/Zeolite Y Catalysts for Alkane Hydroconversion

Lars I. van der Wal, Jogchum Oenema, Luc C. J. Smulders, Nonne J. Samplonius, Karan R. Nandpersad, Jovana Zečević, and Krijn P. de Jong*

Read Online

ACCESS | Metrics & More | Article Recommendations | Supporting Information

ABSTRACT: The preparation of zeolite-based bifunctional catalysts with low noble metal loadings while maintaining optimal performance has been studied. We have deposited 0.03 to 1.0 wt % Pt on zeolite H-USY (Si/Al ~ 30 at./at.) using either platinum(II) tetraammine nitrate (PTA, $Pt(NH_3)_4(NO_3)_2$) or hexachloroplatinic(IV) acid (CPA, $H_2PtCl_6 \cdot 6H_2O$) and studied the nanoscale Pt loading heterogeneities and global hydroconversion performance of the resulting Pt/Y catalysts. Pt/Y samples prepared with PTA and a global Pt loading as low as 0.3 wt % Pt ($n_{Pt}/n_A = 0.08$ mol/mol, where n_{Pt} is the number of Pt surface sites and n_A is the number of acid sites) maintained catalytic performance during *n*-heptane ($T = 210−350$ °C, $P = 10$ bar) as well as *n*-hexadecane ($T = 170−280$ °C, $P = 5$ bar) hydroisomerization similar to a 1.0 wt % Pt sample. For Pt/Y catalysts prepared with CPA, a loading of 0.3 wt % Pt ($n_{Pt}/n_A = 0.08$ mol/mol) sufficed for *n*-heptane hydroisomerization, whereas a detrimental effect on *n*-hexadecane hydroisomerization was observed, in particular undesired secondary cracking occurred to a significant extent. The differences between PTA and CPA are explained by differences in Pt loading per zeolite Y crystal (size ~ 500 nm), shown from extensive transmission electron microscopy energy-dispersive X-ray spectroscopy experiments, whereby *crystal-based n_{Pt}/n_A ratios* could be determined. From earlier studies, it is known that the Al content per crystal of USY varied tremendously and that PTA preferentially is deposited on crystals with higher Al content due to ion-exchange with zeolite protons. Here, we show that this preferential deposition of PTA on Al-rich crystals led to a more constant value of n_{Pt}/n_A ratio from one zeolite crystal to another, which was beneficial for catalytic performance. Use of CPA led to a large variation of Pt loading independent of Al content, giving rise to larger variations of n_{Pt}/n_A ratio from crystal to crystal that negatively affected the catalytic performance. This study thus shows the impact of local metal loading variations at the zeolite crystal scale (nanoscale) caused by different interactions of metal precursors with the zeolite, which are essential to design and synthesize optimal catalysts, in particular at low noble metal loadings.

KEYWORDS: bifunctional catalysts, Pt, zeolite Y, hydroconversion, electron microscopy, energy-dispersive X-ray spectroscopy, nanoscale heterogeneities
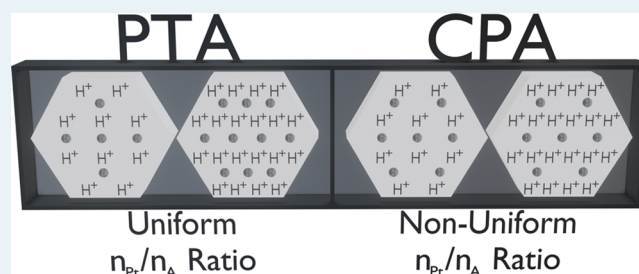
INTRODUCTION

For the production of high-quality fuels and chemicals, which may be based on either fossil or renewable feedstocks, processes such as hydroisomerization and hydrocracking are highly important.[1−6] Hydroisomerization of short-chain paraffins increases the octane number of gasoline by converting *n*-paraffins to *i*-paraffins, whereas hydrocracking produces light hydrocarbons to be used as transportation fuels out of low-value heavy hydrocarbon fractions.[7] A major advantage of hydrocracking over widely applied fluid catalytic cracking processes is that the selectivity of the process towards, for example, the kerosene and diesel fraction or the lighter gasoline fraction can be tuned by adjusting the reaction conditions, providing useful flexibility to the refinery so that the most desired product can be produced at any time.[8]

For the hydroisomerization and hydrocracking processes, metal(sulfide)−zeolite bifunctional catalysts are of major importance.[8,9] Their bifunctionality originates from the presence of metal(sulfide) sites, catalyzing hydrogenation and dehydrogenation of hydrocarbons, and zeolite acid sites, which perform isomerization and cracking reactions. In order to synthesize optimally performing catalysts, think of their activity, selectivity, and stability, various parameters have to

be adjusted, such as the metal loading,[10] the metal to acid site ratio,[10] the metal dispersion to ensure high metal surface area,[11] a homogeneous distribution of the metal nanoparticles over the support,[12] proximity of metal and acid sites,[6,13−15] and the acidity and porosity of the zeolite.[16]

Many of the structural properties and crystallinity of zeolites (micropore size, channel dimensionality, and connectivity) determine the catalytic performance. For hydroisomerization of short-chain paraffins, Pt/mordenite catalysts are widely used, while one of the prominent zeolites for hydrocracking processes is zeolite Y.[17] Zeolite micropores can, however, induce mass transfer limitations, possibly leading to sub-optimal activity and undesired side reactions such as secondary cracking and coke formation.[18−21] To prevent this, post-synthesis treatments have been developed, such as steaming at high temperatures followed by acid leaching to extract Al out of the zeolite framework, resulting in a lower number of acid sites and the formation of intra-crystalline mesopores, thus enhancing the hydrothermal stability and accessibility of the zeolite.[21−25] Furthermore, other techniques have been developed in order to create mesoporosity in zeolites, such as base leaching to remove Si,[26,27] agents that direct mesopore structure formation,[28] and carbon templating.[29]

Additionally, metals as a (de)hydrogenation function have a large impact on the catalytic performance of bifunctional catalysts, as different metals have different intrinsic (de)-hydrogenation activity. Various studies have been investigating the use of catalysts with different metals, ranging from more abundant but less active non-noble metals such as Mo,[19] W,[19] Ni,[30] and Co[31] to the more active but scarce noble metals such as Pt[32,33] and Pd.[32,33] Furthermore, bimetallic catalysts such as NiMo,[34,35] NiW,[36] and Pt−Pd[37] catalysts have been studied, or even trimetallic catalysts such as Pt−Pd−Mg have been investigated.[37] It is known that catalysts containing noble metals, such as Pt and Pd, are significantly more active compared to non-noble metals and are therefore preferred to control hydrocracking and to process sulfur-free feed-stocks.[19,38]

In a bifunctional catalyst, an optimal interplay between the acid and metal active sites, their concentration, strength, and distance is critical for the catalytic performance. In particular, the ratio between the metal and acid sites (n_M/n_A ratio), that is, the amount of metal surface sites and acid sites, averaged at the bulk scale, for example of a catalyst loaded in a laboratory reactor, that has shown to impact the hydrocracking/isomerization reaction mechanism and thus product distribu-tion.[10,39−48] In this context, ideal and non-ideal hydrocracking has been defined, with the ideal hydrocracking indicating that an alkene intermediate undergoes only one isomerization or cracking reaction at an acid site, in between diffusing from a metal dehydrogenation to a metal hydrogenation site.[10,16,39] According to the classical principles postulated by Guisnet et al., for an ideal hydrocracking process, an n_M/n_A ratio of 0.17 or larger (i.e., <6 acid sites per surface metal site) is required.[39] For non-ideal hydrocracking, two regimes have been defined. The first regime is with an n_M/n_A ratio lower than 0.03 where the activity increases with the n_M/n_A ratio, showing that hydrogenation/dehydrogenation is rate limiting. The second regime is in between an n_M/n_A ratio of 0.03 and 0.17, for which the activity is independent of the n_M/n_A ratio, indicating that the acid-catalyzed step is rate limiting, though the stability of the catalyst is limited. These studies were performed with heptane at atmospheric pressure. The findings of later studies

led to a more integral understanding of an "ideal" hydro-cracking process wherein H_2 pressure, hydrocarbon pressure, and temperature were also determining factors.[42]

Metal sites are typically introduced by deposition methods such as ion-exchange (IE) or incipient wetness impregnation (IWI). For the IE method, the zeolite support is immersed in an excess of metal precursor solution under continuous stirring, typically for a couple of hours so that the cations, present as countercharges on the zeolite support, can be exchanged for metal precursor ions. During the IWI method, in contrast to the IE method, the pore volume of the zeolite support is filled with the metal precursor solution. Therefore, the basis of the methods is different, as the IE method is based on an exchange between positively charged precursor ions and zeolite cations such as protons, whereas in the IWI method, the metal is introduced due to the capillary forces acting on the precursor solution.[49]

It is generally accepted that the more homogeneous the metal distribution on the support is, the better the perform-ance of the catalyst is.[49] Previous research on supported metal catalysts has shown that synthesis-originated heterogeneities in the metal loading of catalyst particles or crystals can occur, even within samples of the same batch.[50−53] For IE-prepared Pt/zeolite Y using a cationic $Pt(NH_3)_4^{2+}$ (aq) complex, a clear correlation between Pt loading and Al content of an individual zeolite crystal was observed: a higher Al content led to a higher Pt loading per crystal. The heterogeneities were attributed to different Al contents of the individual zeolite crystals that are directly correlated with the amount of protons and thus exchange sites during the IE method. Even though for platinum(II) tetraammine nitrate (PTA) IWI-prepared sam-ples similar effects were observed, a higher degree of heterogeneity was observed, which was not solely related to Al content. This was as a result of the different principles IWI is based on that may lead to additional heterogeneities, for example already during liquid imbibition.[53] Nevertheless, a similar trend was found: a higher amount of Al led to a higher Pt loading of the crystal in question. This indicated that even during IWI, the proton sites of the zeolites were exchanged for the metal precursor ion, leading to the observed trend.[53]

Likewise, the metal precursor that is used during the synthesis can have an influence on metal heterogeneities on bulk and nanometer scale, which are also known as precursor effects. Each metal precursor has its own characteristics such as decomposition temperature and interaction with the support that affects the metal particle size distribution (PSD) and distribution of metal particles over the support, influencing mainly the local n_M/n_A ratio of the sample. This, as a consequence, can have a large effect on the catalytic performance.[40,54−58] It is therefore important to study the influence of the metal precursor on the synthesis of supported metal catalysts, and the subsequent catalytic performance of the catalyst when different Pt loadings and thus different bulk and local n_M/n_A ratios are in place.

In this study, we focused on the impact of heterogeneities brought about by the use of different Pt precursors on the catalytic performance of Pt/zeolite Y catalysts. Steamed and acid leached zeolite Y was chosen as a support as it is known from previous research that nanoscale metal loading heterogeneities occur and are accessible for transmission electron microscopy energy-dispersive X-ray spectroscopy (TEM−EDX) studies. Furthermore, zeolite Y is widely used in (hydro)cracking of oil fractions and is a useful example to

showcase the influence of nanoscale heterogeneities on catalytic performance in hydroconversion reactions. Two Pt precursors, PTA and CPA, are deposited with different Pt loadings to obtain catalysts with ranging n_{Pt}/n_A ratios to study the influence of different precursors and Pt loadings on the catalytic performance. The latter was investigated via *n*-heptane and *n*-hexadecane hydroconversion to investigate when optimal catalytic performance is obtained for the samples prepared with different precursors and different loadings for hydrocarbons of different molecular weights. It is shown that the PTA- and CPA-prepared samples are similar for higher Pt loadings, though decreasing loadings lead to differences in catalytic performance, due to the differences in nanoscale structures. The latter are nanoscale Pt metal loadings in combination with Si/Al heterogeneities on an individual zeolite crystal level investigated with TEM−EDX. These heterogeneities are assumed to also occur for samples with lower loadings prepared with CPA, indicating that such heterogeneities are influencing catalysis. Thus, by choosing the metal precursor, nanoscale heterogeneities can be controlled, leading to a more uniform n_M/n_A ratio on the nanoscale. It is shown that if and only if we restrict the n_M/n_A heterogeneity, the Pt loading can be decreased significantly without deteriorating the catalytic performance. To the best of our knowledge, this is the first study that links heterogeneities of metal loading at the nanoscale, that is from zeolite crystal to zeolite crystal, to catalytic performance, and is aimed to show the importance of synthesizing a bifunctional catalyst with a more constant n_M/n_A ratio at the nanoscale.

■ METHODOLOGY

Incipient Wetness Impregnation. Ultra-stable zeolite Y (USY, 1 g, previously steamed and acid leached, Zeolyst, CBV760, Si/Al = 30 at./at.) was dried under vacuum overnight in a two-neck round-bottom flask (100 mL) of which one neck was connected to the vacuum pump and the other neck was closed off with a septum. Subsequently, the weight of dry zeolite was determined, while still in the round-bottom flask under vacuum, by weighing the round-bottom flask including the sample under vacuum and subtracting the weight of the empty round-bottom flask under vacuum measured prior to the drying procedure. The Pt precursor, either Pt-$(NH_3)_4(NO_3)_2$ (99.995% trace metal basis) or $H_2PtCl_6 \cdot 6H_2O$ (99.995% trace metal basis), both obtained from Merck, formerly Sigma-Aldrich, was dissolved in demineralized water to obtain a stock solution of Pt precursor (0.14 M for PTA as well as CPA). To obtain the Pt precursor solutions for 0.3 and 0.03 wt % Pt catalysts, the stock solution was diluted 3.3 and 33.3 times, respectively. While the dried material was still under vacuum in the round-bottom flask, the solution was added dropwise to the dried support material with a syringe via the septum up to a volume equal to 90% of the total meso- and micropore volume, which was determined by N_2-physisorption. Thereafter, the impregnated zeolite was magnetically stirred for approximately 30 min while under static vacuum. This was followed by drying at 60 °C for 3 h and drying at 120 °C overnight in a muffle oven in a ceramic dish. Prior to calcination and reduction, the sample was pressed into a tablet, crushed, and sieved to obtain grains of 75−212 μm. Calcination was performed for 2 h under air flow (GHSV = 5000 h^{-1}) at 350 °C (ramp = 0.2 °C/min), followed by reduction for 3 h under pure H_2 flow (GHSV = 2600 h^{-1}) at 600 °C (ramp = 5 °C/min). These were the as-prepared

samples, which were used for all the subsequent measurements. Note that for some measurements, a second pre-treatment was necessary, of which the conditions are specified in the corresponding section.

Ammonia Temperature-Programmed Desorption. Ammonia temperature-programmed desorption (NH$_3$-TPD) was performed on a Micromeritics AutoChem II supplied with a thermal conductivity detector (TCD) calibrated for ammonia. Approximately 100 mg of catalyst was dried in a He flow for 1 h at 600 °C (ramp 10 °C/min). Subsequently, the temperature was decreased to 100 °C, after which ammonia (10 vol % in He) was adsorbed pulsewise until oversaturation occurred. Physisorbed ammonia was removed by flowing He for 2 h at 100 °C. Subsequently, ammonia desorption was measured until 600 °C (ramp 10 °C/min). The obtained results were quantified by deconvolution of the TCD signal with three Gaussian functions since the high-temperature desorption peak had a shoulder due to delayed desorption of NH$_3$.

Fourier Transform Infrared Spectroscopy. Fourier transform infrared (FT-IR) spectroscopy was performed in transmission mode on a Thermo iS5 instrument. The instrument was equipped with a DTGS detector, and 16 scans per spectrum were taken with a resolution of 4 cm^{-1}. Approximately 15 mg of sample was pressed into a self-supported wafer, which was then placed in a well-sealed cell with calcium fluoride windows. This allowed switching between vacuum and probe molecule vapor. The samples were first dried under high vacuum at 550 °C (ramp 10 °C/min) and kept at this temperature for 2 h. When the cell had a temperature of 30 to 40 °C, a spectrum was recorded after which pyridine (Sigma-Aldrich, 99.8%, probe molecule) was introduced, at a pressure of 7−8 mbar, to adsorb on the sample for 20−25 min, while spectra were recorded every 2 min starting at minute 1. This was followed by the desorption of pyridine by applying a high vacuum for 30 min, after which the temperature was increased to 150 °C (ramp 2 °C/min) and maintained at this point for 30 min after which a spectrum was collected that was used for the assessment of the acidity of the samples. Quantification of the acid sites was performed by band integration of the peaks at 1544 cm^{-1} (Brønsted acid sites) and 1455 cm^{-1} (Lewis acid sites), where a correction was performed for the specific molar absorption coefficient and the mass and the radius of the wafer. Apparent integral absorption coefficients of 1.67 cm/μmol (Brønsted acid sites) and 2.22 cm/μmol (Lewis acid sites) were used for the quantification.[59−61]

Hydrogen Chemisorption. Hydrogen chemisorption measurements were carried out on a Micromeritics ASAP 2020C device. First, the samples were reduced at 300 °C in flowing H$_2$ for 1 h. Subsequently, the samples were evacuated at 300 °C. Thereafter, the H$_2$ uptake was measured at 35 °C. For calculating the average particle size, the following assumptions were made: (hemi)spherical particles are present, an H/Pt$_s$ stoichiometry of 1, and an atomic cross section for Pt surface atoms of 0.08 nm^2.

Nitrogen Physisorption. Nitrogen physisorption isotherms were measured at −196 °C using a Micromeritics TriStar II Plus apparatus. Prior to analysis, the samples were dried overnight under a N$_2$ flow at 300 °C. Accessible surface areas were determined using the Brunauer−Emmett−Teller (BET) method by curve fitting at monolayer adsorption. The micropore (<2 nm) volumes were based on a *t*-plot analysis

using a Harkins−Jura thickness curve fitted between 0.35 and 0.50 nm thickness. The total pore volumes were derived from the amount of N_2 adsorbed at $p/p_0 = 0.95$. The pore size distributions were determined via the Barrett−Joyner−Halenda analysis from the desorption isotherm using the Harkins−Jura thickness curve.

Transmission Electron Microscopy. TEM measurements were performed on a Talos F200X equipped with an X-FEG electron source and operated at 200 kV. Images were acquired in scanning transmission electron microscopy (STEM) mode using a high-angle annular dark-field (HAADF) detector with a frame time of 20 s. Number-averaged Pt particle sizes were obtained by measuring at least 500 Pt nanoparticles per sample. The surface-averaged particle size was determined by the following formula: $d_s = \sqrt{\left(\frac{1}{N}\sum_{N=1}^{N} d_i^2\right)}$, where d_S is the surface-averaged particle size, d_i is the diameter of a Pt particle, and N is the total number of particles counted. Based on the obtained surface-averaged particle size, dispersions were determined following previous research on Pt metal nanoparticle dispersion related to Pt metal nanoparticle size.[11] Subsequently, with the obtained dispersion and the Pt wt % obtained via elemental analysis [inductively coupled plasma (ICP)], we calculated the amount of atoms at the surface available for catalysis.

Energy-Dispersive X-ray Spectroscopy. EDX measurements were performed in TEM mode. For individual crystal TEM−EDX spectra, the beam was spread around one zeolite crystal at a time without irradiating the other material. TIA software was used to collect the spectra, with an acquisition time of 10 min. Subsequent quantification was performed with ES Vision software. The background was corrected manually, while automatic peak identification by the software was performed. Thereafter, quantification to atomic ratios was performed with the Cliff−Lorimer technique. The quantification results of these individual zeolite crystal EDX spectra were visualized in graphs, where the Pt/(Si + Al) atomic ratio was plotted versus the Al/(Si + Al) atomic ratio. Finally, the results were fitted with a linear function, $y = a + bx$, where a (intercept) and b (slope) are variables, in order to fit the obtained results as optimally as possible.

X-ray Diffraction. X-ray diffraction (XRD) measurements were performed on a Bruker-AXS D2 Phaser X-ray diffractometer in the Bragg−Brentano mode equipped with a Lynxeye detector (Co K$\alpha_{1,2}$, λ = 1.790 Å). Prior to the recordings, the samples were crushed into a fine powder. Diffractograms were recorded between 6 and 40° 2θ under a constant rotation of 15 rpm.

n-Heptane (n-C₇) Hydroisomerization. n-Heptane (n-C₇) hydroisomerization was used as a model reaction for the investigation of the hydroisomerization of a short hydrocarbon. The catalytic tests were executed on an Avantium Flowrence with 16 parallel fixed bed reactors (internal diameter = 2 mm). The catalyst (25 mg, sieved in a particle size sieve fraction of 75−212 μm) was loaded in each reactor and reduced in situ at 300 °C for 2 h (ramp 5 °C/min) in a 25% H_2/He flow. The n-C₇ hydroisomerization (Acros Organics, 99+% pure) catalytic test was done for 160 h with an H_2/n-C₇ mole ratio of 10, a feed rate for n-C₇ of 2 $g_{n\text{-}C_7} \cdot g_{cat}^{-1} \cdot h^{-1}$, and a total pressure of 10 bar. The following gasses, used during the catalytic test, were obtained from Linde gas: He 5.0, N_2 5.0, and H_2 6.0. Helium was used as an internal standard and N_2 as a diluent. During

catalysis, the product stream was heated at 150 °C and diluted with N_2 to prevent product condensation and was analyzed online with an Agilent 7890A gas chromatograph. The hydrocarbon products were analyzed on an Agilent J&W PoraBOND Q column connected to an FID. Measurements were conducted in a temperature range from 210 to 350 °C. At each temperature, two gas chromatography (GC) measurements were performed under identical conditions. The average of these GC measurements was used for the activity and selectivity plots (uncertainty ≤ 1%). To assess the stability of the catalyst after the highest temperature to which the catalyst was exposed, the temperature was decreased to 270 °C and the catalytic performance was measured (the so-called backcheck). The activity is expressed as the percentage of converted C₇ ($X_{n\text{-}C_7}$), calculated as follows, where F stands for the flow of the specified molecule

$$X_{n\text{-}C_7} = \left(1 - \frac{F_{C\,wt\,n\text{-}C_7,out}}{F_{C\,wt\,n\text{-}C_7,in}}\right) \cdot 100\% \tag{1}$$

The C₇ isomer selectivity ($S_{i\text{-}C_7}$) and yield ($Y_{i\text{-}C_7}$) were determined as follows

$$S_{i\text{-}C_7} = \left(\frac{F_{C\,wt\,i\text{-}C_7,out}}{F_{C\,wt\,n\text{-}C_7,in} - F_{C\,wt\,n\text{-}C_7,out}}\right) \cdot 100\% \tag{2}$$

$$Y_{i\text{-}C_7} = \left(\frac{F_{C\,wt\,i\text{-}C_7,out}}{F_{C\,wt\,n\text{-}C_7,in}}\right) \cdot 100\% \tag{3}$$

The yield of cracked products ($Y_{C_3+C_4}$) was determined by the following formula

$$Y_{C_3+C_4} = \left(\frac{F_{C\,wt\,C_3,out} + F_{C\,wt\,C_4,out}}{F_{C\,wt\,n\text{-}C_7,in}}\right) \cdot 100\% \tag{4}$$

n-Hexadecane (n-C₁₆) Hydroisomerization. n-Hexadecane (n-C₁₆) hydroisomerization was used as a model reaction for the investigation of the hydroisomerization of a long hydrocarbon. The catalytic tests were executed on an Avantium Flowrence with 16 parallel fixed bed reactors (internal diameter = 2 mm). The catalyst (25 mg, sieved in a particle size fraction of 75−212 μm) was loaded in a reactor and reduced in situ at 300 °C for 2 h (ramp 5 °C/min) in a H_2 flow. The n-C₁₆ hydroisomerization (Acros Organics, 99% pure) catalysis was done for 220 h with an H_2/n-C₁₆ mole ratio of 10, a feed rate for n-C₁₆ of 2 $g_{n\text{-}C_{16}} \cdot g_{cat}^{-1} \cdot h^{-1}$, and a total pressure of 5 bar. The following gasses, used during the catalytic test, were obtained from Linde gas: He 5.0, N_2 5.0, and H_2 6.0. Helium was used as an internal standard and N_2 as a diluent. During catalysis, the product stream was heated at 200 °C and diluted with N_2 to prevent product condensation and was analyzed online with an Agilent 7890B gas chromatograph. The hydrocarbon products were analyzed on an Agilent HP PONA 50m connected to an FID. Measurements were conducted in a temperature range from 170 to 280 °C. At each temperature, two GC measurements were performed under identical conditions. The average of these GC measurements was used for the activity and selectivity plots (uncertainty ≤ 3%). To assess the stability of the catalyst after the highest temperature to which the catalyst was exposed, the temperature was decreased to 210 °C and the

Table 1. General Properties of the Pt/H−Y Catalysts

sample	ICP (wt % Pt)	d_N TEM (nm)	d_S TEM (nm)	dispersion	Pt surface atoms (mmol/g_{cat}) (n_{Pt})	d_S H$_2$-chem (nm)	micropore volume (mL/g)^a	Brønsted acidity (mmol/g) (n_A)^b	metal to acid site ratio (n_{Pt}/n_A, mol/mol)^c
PTA−1.0wt%Pt	1.0	1.5 ± 0.6	1.6 ± 0.6	0.76	0.039	1.8	0.27	0.13	0.30
PTA−0.3wt%Pt	0.3	1.4 ± 0.7	1.6 ± 0.7	0.76	0.012	n.d.^{e}	0.26	0.14	0.08
PTA−0.03wt%Pt	0.05	n.d.	n.d.	1.0^d	0.002	n.d.^{e}	0.27	0.14	0.01
CPA−1.0wt%Pt	0.9	1.6 ± 0.4	1.6 ± 0.4	0.76	0.035	2.2	0.27	0.12	0.29
CPA−0.3wt%Pt	0.3	1.9 ± 0.9	2.1 ± 0.9	0.65	0.010	n.d.^{e}	0.26	0.13	0.08
CPA−0.03wt%Pt	0.06	n.d.	n.d.	1.0^d	0.002	n.d.^{e}	0.27	0.13	0.01

^{a}The micropore volume of pristine zeolite Y as comparison is 0.27 mL/g. ^{b}The Brønsted acidity of pristine zeolite Y as comparison is 0.12 mmol/g. ^{c}Based on the available Pt sites determined with TEM and Brønsted acid sites determined with pyridine FT-IR. ^{d}Assumed that Pt metal atoms are 100% accessible. ^{e}Not measured as the measurement would be inaccurate at these low loadings.

catalytic performance was measured (backcheck). The activity is determined as the percentage of converted C$_{16}$ ($X_{n-C_{16}}$) calculated as follows

$$X_{n-C_{16}} = \left(1 - \frac{F_{C\,wt\,n-C_{16},out}}{F_{C\,wt\,n-C_{16},in}}\right) \cdot 100\% \quad (5)$$

The C$_{16}$ isomer selectivity ($S_{i-C_{16}}$) and yield ($Y_{i-C_{16}}$) were determined as follows

$$S_{i-C_{16}} = \left(\frac{F_{C\,wt\,i-C_{16},out}}{F_{C\,wt\,n-C_{16},in} - F_{C\,wt\,n-C_{16},out}}\right) \cdot 100\% \quad (6)$$

$$Y_{i-C_{16}} = \left(\frac{F_{C\,wt\,i-C_{16},out}}{F_{C\,wt\,n-C_{16},in}}\right) \cdot 100\% \quad (7)$$

The yield of cracked products ($Y_{Cracked\ products}$) was determined by the following formula

$$Y_{cracked\ products} = \left(\frac{F_{C\,wt\,C_{1-14},out}}{F_{C\,wt\,n-C_{16},in}}\right) \cdot 100\% \quad (8)$$

For the cracking product distribution patterns of n-hexadecane hydroisomerization, the yield of individual cracked products in mol % (Y_{C_m}; $m = 1-14$) was calculated by

$$Y_{C_m} = \left(\frac{F_{C\cdot C_m,out}}{F_{C\cdot nC_{16},in}}\right)\left(\frac{16}{m}\right) \cdot 100\% \quad (9)$$

■ RESULTS AND DISCUSSION

The series of Pt on mesoporous zeolite Y (USY, Zeolyst, CBV760) catalysts with either 1.0, 0.3, or 0.03 wt % Pt loading were synthesized by IWI using either PTA (Pt(NH$_3$)$_4$(NO$_3$)$_2$) or CPA (H$_2$PtCl$_6$·6H$_2$O) precursor. The Pt weight loadings were determined with ICP optical emission spectroscopy (ICP−OES), summarized in Table 1. The weight loadings determined with ICP−OES corresponded to the aimed 1.0 and 0.3 wt % of Pt. In the case of 0.03 wt % Pt samples, ICP showed slightly higher loading than aimed for, likely because the measurement error is too large for a reliable determination at these low loadings. Since the samples were prepared via impregnation techniques, which led to full metal uptake, and the weight loadings for the samples with higher loadings were similar to the projected weight loadings, it was assumed that the samples with an aimed Pt loading of 0.03 wt % had that amount of Pt.

Subsequently, high-angle annular dark-field scanning transmission electron microscopy (HAADF-STEM) measurements were performed to image Pt metal nanoparticles on the zeolite support and to determine PSDs. Figure 1 shows the representative HAADF-STEM images for the PTA and CPA prepared samples as well as their PSD. For the samples with 0.03 wt % Pt, however, PSD histograms were not obtained since only few particles were observed during TEM measurements and most likely the majority of Pt was present as atomically dispersed Pt or clusters of a few Pt atoms. For these samples, a dispersion of 100% was assumed, as no large Pt metal nanoparticles were observed during TEM studies. For the samples with 1.0 wt % Pt loadings, it is observed that the PSD is rather narrow, irrespective of the precursor, with the majority of particles below 3 nm. The samples with 0.3 wt % Pt showed slightly different PSD, with the CPA-prepared sample showing a broader distribution, which, at these low loading, could possibly influence the catalytic performance. One might expect that PTA-prepared samples would have a higher dispersion after impregnation as [Pt(NH$_3$)$_4$]$^{2+}$ can be exchanged with zeolite proton sites, resulting in a strong interaction with the zeolite support. The [PtCl$_6$]$^{2-}$ anion of CPA cannot be exchanged with these proton sites, and therefore this strong interaction with the zeolite support is absent. During heat treatment, however, the Pt precursor ions have different mobilities. In microporous zeolite structures, water vapor is present during heat treatment, which can lead to increased mobility of the platinum cations resulting in large Pt particles when [Pt(NH$_3$)$_4$]$^{2+}$ is used.[11,62−64] For the H$_2$PtCl$_6$ precursor, the Pt, Cl, and O start interacting with each other at 300 °C already during a calcination procedure, resulting in the formation of oxychloroplatinum species, which favor the formation of small metal nanoparticles.[65−67] This eventually results in catalysts with similar particle sizes even when synthesized with a different Pt precursor, especially since particle growth is restricted by the zeolite micropores. The surface-averaged particle size was also determined from TEM (see the Methodology for detailed information) and compared with H$_2$-chemisorption-derived particle diameters (Table 1). Since the H$_2$ chemisorption showed particle size similar to those from HAADF-STEM, obtained by analyzing the Pt nanoparticle size on a number of zeolite crystals, the latter was considered relevant for the entire sample.

In order to investigate the impact of catalyst preparation on the crystallinity and pore structure, XRD measurements and N$_2$-physisorption measurements were performed, respectively. XRD (Supporting Information Figure S1) showed that identical XRD patterns with similar intensities were obtained, indicating that the crystal structure was retained during catalyst
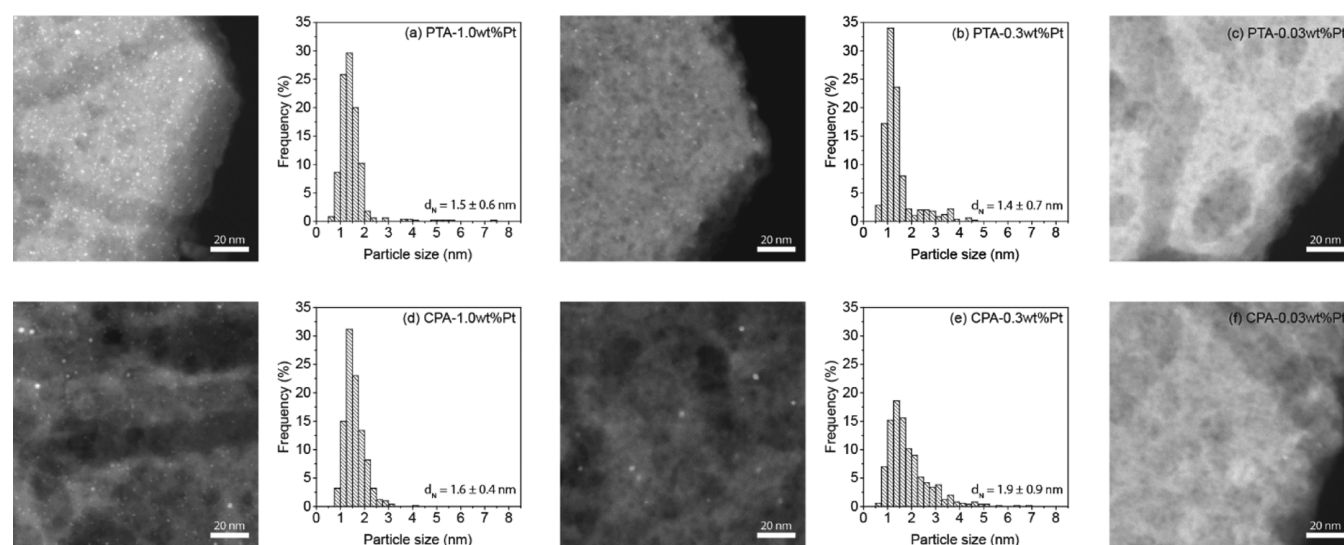
Figure 1. HAADF-STEM images, particle size histograms, and number-averaged particle sizes of samples prepared with PTA (a–c) and CPA (d–f). (a) PTA−1.0wt%Pt, (b) PTA−0.3wt%Pt, (c) PTA−0.03wt%Pt, (d) CPA−1.0wt%Pt, (e) CPA−0.3wt%Pt, and (f) CPA−0.03wt%Pt. Scale bars are 20 nm.

synthesis. N_2-physisorption (Table 1 and Supporting Information Figure S2 and Table S1) shows similar N_2-physisorption isotherms and thus similar micropore volumes, total pore volumes, and BET specific surface areas of the samples with Pt deposited on zeolite Y compared to pristine zeolite Y. These results show that the pore structure was identical with pristine zeolite Y, and therefore, it can be stated that the integral structure of the zeolite did not change during the synthesis of all the bifunctional catalysts.

NH_3-TPD measurements were performed to determine the total acidity of the synthesized Pt/zeolite Y catalysts (Table 1 and Supporting Information Figure S3 and Table S2). It is shown that the total acidity was similar for Pt/zeolite Y catalysts as compared to pristine zeolite Y. Only minor differences between the samples were observed within the error of these measurements. For all samples, the percentage of strong acid sites ranged from 70 to 75%, whereas the percentage of weak acid sites ranged from 25 to 30%, as determined by deconvolution of the NH_3-TPD signal.

Previous research has already shown that it is important to know the ratio between the two active sites, namely metal and (Brønsted) acid sites (n_{Pt}/n_A). As this information cannot be obtained from NH_3-TPD measurements, pyridine FT-IR measurements were performed for pristine zeolite Y as well as for the Pt/zeolite Y samples (Supporting Information Figure S4 and Table S3). Five different vibrations in the region of interest can be identified, of which the vibrational band at 1544 cm^{-1} is attributed to pyridinium ions formed on Brønsted acid sites and the vibrational band at 1455 cm^{-1} is attributed to pyridine coordinated to Lewis acid sites.[59−61] The amount of Brønsted acid sites was 0.13 ± 0.01 mmol/g for the obtained catalysts and the ratio between Brønsted and Lewis acid sites was similar (Table 1 and Supporting Information Table S3). This indicated that the synthesis method and the deposition of the Pt metal did not have a noticeable influence on the acidity of the zeolite support.

It should be mentioned that the measured total acidity for NH_3-TPD (0.32 mmol/g) and pyridine FT-IR (0.19 mmol/g) was significantly lower than the theoretical total acidity based on the Al-content of the zeolite (0.54 mmol/g). This is mainly

attributed to the presence of extra-framework Al species, which is well known for commercially available ultra-stable zeolite Y (CBV760), which do not lead to Brønsted acid sites.[68−70] Moreover, there is a significant discrepancy between the total acidity obtained with NH_3-TPD (0.32 mmol/g) and pyridine FT-IR (0.19 mmol/g), which is attributed to the different molecular sizes of the probe molecules, as the NH_3 molecule can probe the acid sites in smaller pores.[71] Additionally, as NH_3 adsorption occurred at 100 °C versus pyridine FT-IR performed at 150 °C, in combination with difference in base strength, NH_3 probed an additional number of acid sites that have a weaker strength, compared to pyridine FT-IR.[61] Hereafter, the Brønsted acidity determined with pyridine FT-IR was used for the determination of the metal to acid site ratio. This ratio was calculated by the use of the available Pt surface atoms (as derived from TEM measurements and Pt loading) and the amount of Brønsted acid sites (as determined with pyridine FT-IR) for all catalysts (Table 1). We note that the samples with 1.0 wt % Pt had an n_{Pt}/n_A ratio above 0.17 and that samples prepared with different precursors but similar loadings had similar n_{Pt}/n_A ratios.

Previous research had already shown that there is a large variation in Pt loading of individual zeolite crystals within the same catalyst prepared either with ion-exchange or IWI using PTA.[53] These were related to preexisting heterogeneities in Al content (thus proton sites for exchange with a positively charged $[Pt(NH_3)_4]^{2+}$ ion) per zeolite crystal likely as a result of post-synthesis treatments used for mesopore formation.[53] For the IWI-prepared samples using PTA, the data was more scattered due to factors such as depletion of Pt from the precursor solution by crystals that first come in contact with the solution or insufficient mixing during IWI, but still the dependence of metal loading on aluminum content was undeniable.[53] Here, we hypothesized that this could also be the case for the PTA-prepared samples in this research, but the conclusion would not hold for CPA-prepared samples as the CPA precursor is negatively charged and therefore does not have such an attractive interaction with the negatively charged zeolite framework as the PTA does. To investigate this, quantitative TEM−EDX measurements of individual zeolite

crystals, which were approximately 500 nm in size (Supporting Information Figure S5), in the same sample batch, were performed for the 1.0 wt % Pt samples (Figure 2). TEM−EDX measurements of samples with 0.3 and 0.03 wt % Pt were omitted, as the loadings are rather low, resulting in large measurement errors.

Figure 2 illustrates the increase in Pt loading per zeolite crystal as a function of the Al content for said crystal for the PTA 1.0 wt % sample, where plotting the linear relationship between Pt content and Al content of the zeolite crystal was based on previous research, showing the linear relationship between the two mentioned parameters.[53] The data is scattered, but the correlation between metal loading and aluminum content is clear. Furthermore, it was assumed that the Brønsted acidity scaled with the $Al/(Si + Al)$ ratio, as it was previously shown that extra-framework Al did not reside in the zeolite crystals but was present as alumina-rich clusters within the sample.[53] Thus, this linear relationship suggests that the n_{Pt}/n_A ratio is rather constant (equal to 0.10 at./at. ± 0.02) throughout the sample even at the nanoscale. Please note that the local average n_{Pt}/n_A ratio is lower than the bulk ratio for this sample, namely, an n_{Pt}/n_A ratio of 0.30 at./at. Various reasons, such as not all Pt is detected with TEM−EDX and that all Al is measured while not every Al species accounts for one acid site among others, could be put forward. Additionally, the bulk n_{Pt}/n_A ratio is calculated with the amount of Brønsted acid sites determined with pyridine FT-IR, which as explained before underestimates the acidity of the samples. For the CPA−1.0wt%Pt sample, a similar fit was performed, which led to a horizontal line, and is shown to guide the eye and to illustrate the fundamental difference between PTA- and CPA-prepared samples. Therefore, while large heterogeneities in Pt loading were observed, for CPA they appeared not to be correlated with the Al content of the individual zeolite crystals. No Pt−Al correlation is to be expected as no electrostatic interaction between the CPA anion and the zeolite occurs, while the large scattering in the data reflects the drawback of IWI, whereby metal is not always uniformly distributed throughout the zeolite powder.[49,52,53] As a consequence, significant deviation of n_{Pt}/n_A ratio on a nanometer scale is revealed by quantification of TEM−EDX measurements of individual crystals (0.10 at./at. ± 0.06).
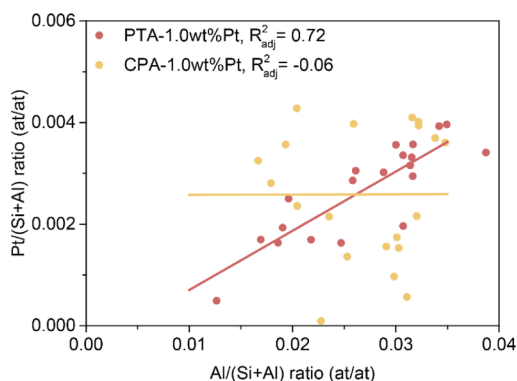

Figure 2. Quantification of individual crystal EDX spectra for the 1.0 wt % Pt samples. A clear correlation between the Al content of an individual crystal and the Pt loading of that crystal is observed for the PTA sample, whereas there is no correlation for the CPA-prepared sample.

One could argue that EDX might not be the most suitable technique to study these phenomena, as it is a very localized technique. As our zeolite crystals were 500 nm in size, electrons can easily penetrate the whole crystal and therefore lead to EDX signals from the entire crystal. It should however be mentioned that the $Al/(Si + Al)$ atomic ratio and the $Pt/(Si + Al)$ atomic ratio measured with individual crystal TEM−EDX is 15−20% lower compared to the nominal bulk value (Supporting Information Table S4). The possible reasons could be that not all Pt is detected or the presence of extra-framework Al in the zeolite sample, which is well known for commercially available zeolite Y (CBV760),[68−70] not leading to acid sites on which the nominal bulk value is based. Despite the underestimation of $Al/(Si + Al)$ and $Pt/(Si + Al)$, the technique has shown to be sensitive enough to detect differences in Pt loadings even at metal loadings of 1.0 wt % Pt and is therefore deemed suitable for detailed nanoscale analysis.[53]

To study the impact of Pt loading and distribution on the catalytic performance, catalysts were first investigated for hydroisomerization of n-heptane (Acros Organics, 99+% pure) as a model short-chain-length feedstock. For this purpose, 25 mg of the 75−212 μm catalyst grains was loaded in a reactor. Note that at these grain sizes, internal diffusion limitations were absent according to the Weisz−Prater criterion (see the Supporting Information for details).[72−75] The activity as well as the selectivity plots are shown in Figure 3. The activities of PTA−1.0wt%Pt and PTA−0.3wt%Pt were nearly identical, indicating that the n_{Pt}/n_A ratio can be significantly reduced below 0.17 without losing the catalyst activity. For CPA-prepared samples, reducing the Pt loading from 1.0 to 0.3 wt % led to a negligible decrease in activity, indicating that for samples prepared with CPA, the Pt wt % loading can also be reduced, without significant loss of the activity. However, a decrease to 0.03 wt % Pt, for PTA- as well as CPA-prepared samples, led to a more pronounced decrease in activity. Interestingly, selectivity toward isomers, of which the majority is monobranched and only a small part (max 10%) is dibranched (Supporting Information Figure S6), not only remained the same but even increased slightly when the Pt loading was reduced to 0.3 wt % (Figure 3b,d). These differences are, however, minor and can be attributed to metal-catalyzed reactions as noted in previous studies.[76,77] The main mechanism occurring is the classical bifunctional mechanism; however, the product distributions of all samples (Supporting Information Figures S7 and S8) suggest that the bimolecular mechanisms as described by Blomsma et al. has occurred to a limited but noticeable extent.[32,77−79] The details of the metal-catalyzed reactions and the bimolecular mechanism can be found elsewhere and are outside the scope of this study.[32,76−79]

After the temperature ramp, the stability of the catalysts was checked by performing a backcheck at 270 °C, where the activity and selectivity were compared to the measurements during the temperature ramp (Supporting Information Table S5). It can be seen that only the 0.03 wt % Pt samples for PTA- as well as CPA-prepared samples showed a decreased activity and selectivity to isomers during the backcheck as compared to during the temperature ramp. This can be explained by the fact that less Pt is available for hydrogenation of olefinic species. These olefinic species can subsequently oligomerize, resulting in coke formation, which leads to deactivation of acid sites and only happens at low Pt loadings. Additionally, it should be mentioned that Pt particle size did not increase during catalysis
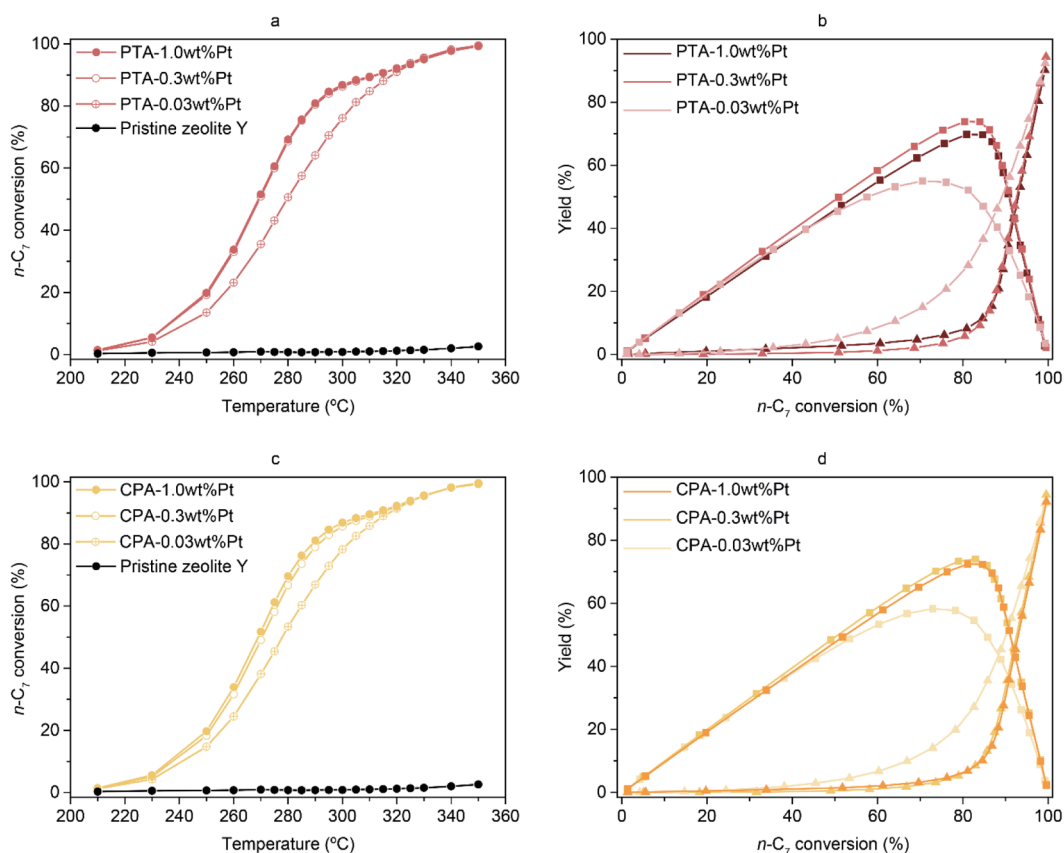
Figure 3. Activity and selectivity plots for *n*-heptane isomerization for PTA-prepared samples (a + b) and CPA-prepared samples (c + d). (b,d) give the yield of isomerized products (■) as well as cracked products (▲). Catalytic tests were performed with a mole ratio of 10 for H_2/n-C_7, a feed rate for *n*-C_7 of 2 $g_{n-C_7} \cdot g_{cat}^{-1} \cdot h^{-1}$, and a total pressure of 10 bar.

for the 1.0 wt % and 0.3 wt % Pt samples as shown from HAADF-STEM image analysis of fresh and used catalysts (Supporting Information Figure S9).

To further investigate the influence of hydrocarbon chain length on the catalytic activity and selectivity, *n*-hexadecane hydroisomerization was performed. The results are shown in Figure 4. It is clear that for PTA, a decrease from 1.0 wt % Pt to 0.3 wt % Pt did not lead to a decrease in activity (Figure 4a). This is in contrast to CPA-prepared samples, where the decrease from 1.0 wt % Pt to 0.3 wt % Pt led to a drop in activity (Figure 4c). Decreasing the Pt loading further to 0.03 wt % Pt led to an almost inactive material for PTA- as well as CPA-prepared samples. Thus, clearly for the hydroisomerization of a larger hydrocarbon, the metal loading, and the related (nanoscale) n_{Pt}/n_A ratio, becomes more critical to obtain the desired product.

Decreasing the Pt loading from 1.0 to 0.3 wt % led to a decrease in isomerization selectivity (sum of monobranched and multibranched *i*-C_{16}) for CPA-based Pt/Y catalysts. For PTA, the maximum isomer yield was 39% for the 1.0 wt % Pt catalyst and 35% for the 0.3 wt % Pt catalyst and deemed similar. For CPA-prepared samples, there was a significant decrease from 40% to 20% isomer yield upon decreasing the metal loading from 1.0 wt % Pt to 0.3 wt % Pt. This is in contrast to what was shown for *n*-C_7 hydroisomerization, where the 0.3 wt % Pt samples had a similar selectivity for *i*-C_7 as the 1.0 wt % Pt samples for PTA- as well as CPA-prepared samples. Thus, for reactions for these kinds of studies, it is important that larger hydrocarbons are also used in order to be

able to note subtle differences between catalysts, such as nanoscale heterogeneities. Such heterogeneities clearly have a more significant influence as cracking of larger hydrocarbons is more affected by heterogeneity of the n_{Pt}/n_A ratio at the nanoscale.

Stability tests after the temperature ramp were also performed for *n*-C_{16} hydroisomerization by decreasing the temperature to 210 °C (Supporting Information Table S6). It can be observed that now all catalysts showed a significant decrease in activity as well as in isomer selectivity due to the deactivation of the catalyst most likely due to coke formation, which blocks the active sites. The 1.0 wt % Pt and the 0.03 wt % Pt samples behaved in a similar way irrespective of being synthesized with PTA or CPA. The main difference came with the 0.3 wt % Pt samples, where for PTA, the activity and selectivity decrease of the 0.3 wt % Pt sample was similar to the 1.0 wt % Pt sample, while this was clearly not the case for the CPA-prepared sample, which had an activity and selectivity similar to the 0.03 wt % Pt sample during the backcheck. This underlines the importance of a uniform n_{Pt}/n_A ratio on a crystal basis. If the local n_{Pt}/n_A ratio is heterogeneous, the chance of oligomerization on acid sites increases, resulting in the formation of coke, which blocks the active sites. This explains the severe activity and selectivity decrease for the 0.3 wt % Pt sample prepared with CPA with a heterogeneous n_{Pt}/n_A ratio, while this decrease is absent for the 0.3 wt % Pt sample prepared with PTA as it has a uniform n_{Pt}/n_A ratio.

The distribution of cracking products during *n*-C_{16} hydroconversion was determined at 35% cracking yield (Figure 5)
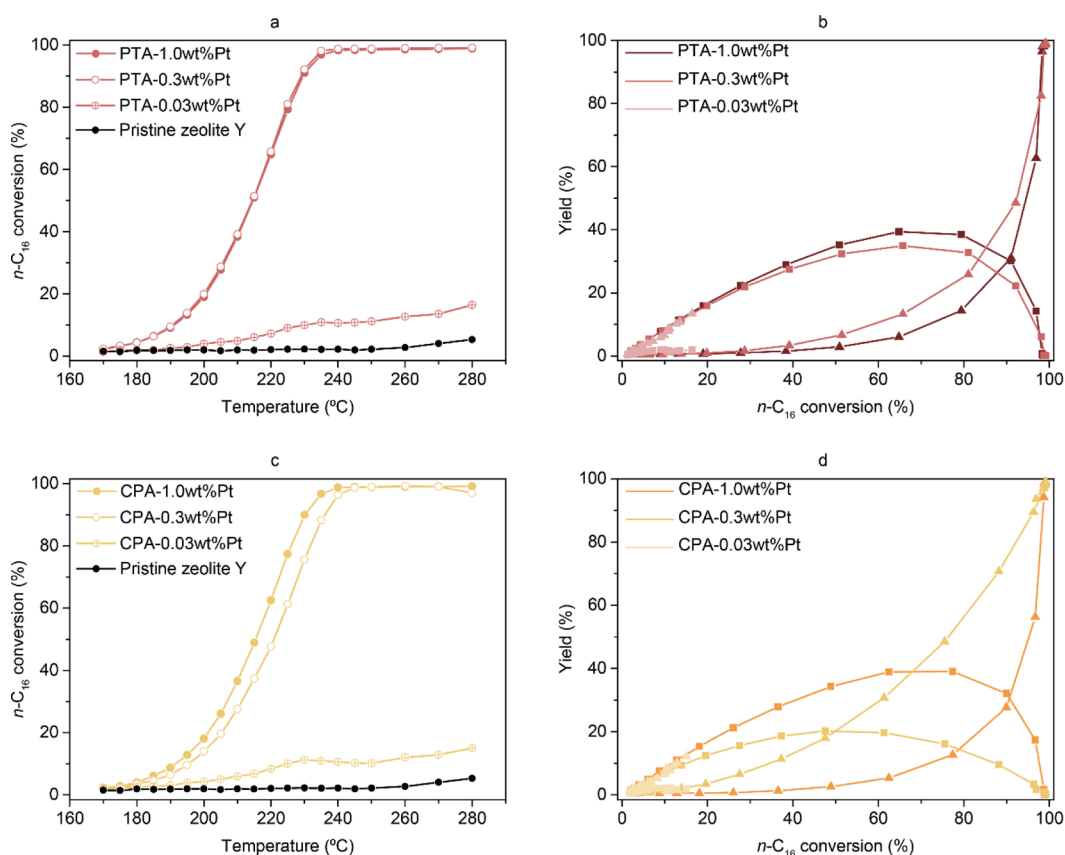
Figure 4. Activity and selectivity plots for *n*-hexadecane isomerization for PTA-prepared samples (a + b) and CPA-prepared samples (c + d). (b,d) Yield of isomerized products (■) as well as cracked products (▲). Catalytic tests were performed with a mole ratio of 10 for $H_2/n\text{-}C_{16}$, a feed rate for $n\text{-}C_{16}$ of 2 $g_{n\text{-}C_{16}} \cdot g_{cat}^{-1} \cdot h^{-1}$, and a total pressure of 5 bar.
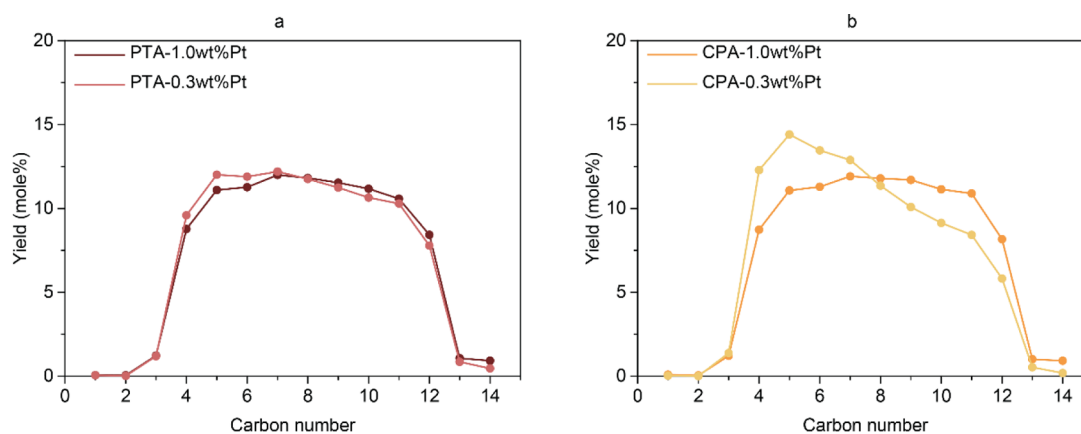

Figure 5. Carbon distribution of cracked products at 35% cracking yield of *n*-hexadecane in mole % for PTA (a) and CPA (b).

for the 1.0 and 0.3 wt % samples. If only primary cracking occurs, a symmetrical distribution of the mole % of hydrocarbons is expected, which is true for both 1.0 wt % samples and for the 0.3 wt % sample prepared with PTA. Therefore, in the case of PTA, the Pt weight loading can be decreased to 0.3 wt % Pt without the occurrence of undesired secondary cracking. For the 0.3 wt % sample prepared with CPA, more of the smaller hydrocarbons (<C_7) are produced, indicating that secondary cracking of cracked products occurred. This is most often an undesired side reaction, as one ends up with more smaller (C_3, C_4) hydrocarbons and less transportation fuel. The reason for the difference in catalytic

performance between $n\text{-}C_7$ and $n\text{-}C_{16}$ has most likely to do with their molecular size, as the cross-sectional area for $n\text{-}C_7$ is 0.57 nm^2 and the effective cross-sectional area for $n\text{-}C_{16}$ was estimated as 1.10 nm^2.[80−82] Compared to the cross-sectional areas of the pore entrances (0.50 nm^2) and the pore cavities (1.13 nm^2) this is a large difference and indicates that $n\text{-}C_{16}$ will diffuse much slower through the zeolite micropores than n-C_7. This is also indicated in previous research by Thybaut et al., who have shown that a higher reactant carbon number leads to more non-ideal hydrocracking since the rate coefficient for acid-catalyzed reactions increases with the carbon number.[42] When this is correlated with uniform versus non-
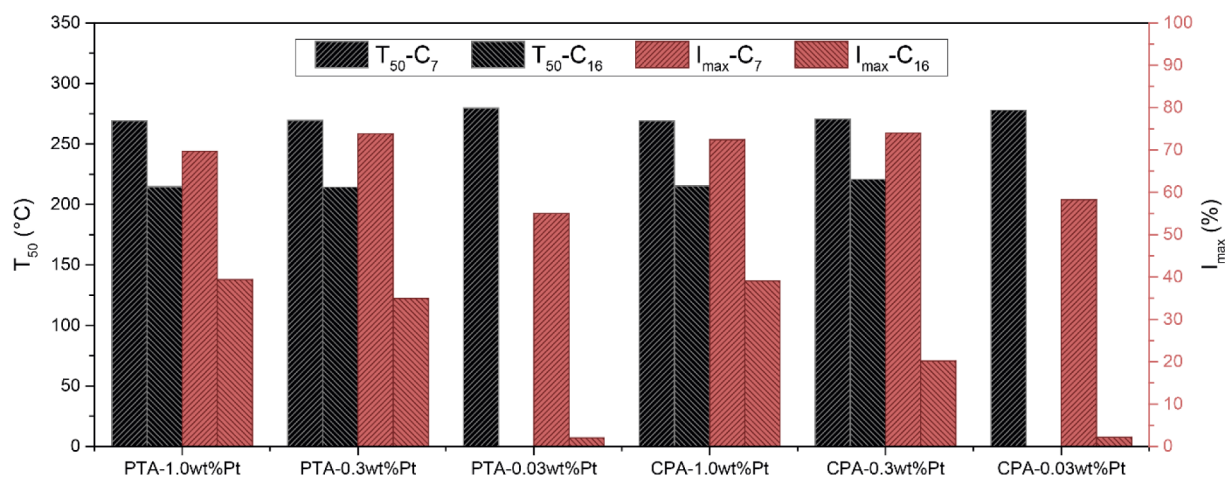
Figure 6. Summary of the isomerization reactions to compare the obtained results more easily. Shown are the temperature to reach 50% conversion (T_{50}) on the left axis and the maximum isomer yield (I_{max}) on the right axis.

uniform nanoscale metal to acid site ratios, the following is hypothesized. Shorter hydrocarbons can diffuse faster through the zeolite micropores, and therefore the chance for secondary cracking reactions decreases. When a larger hydrocarbon is used, diffusion through the zeolite micropores is slower, which increases the chance of, for example, secondary cracking. Therefore, it is more desirable to have the metal and acid sites concurrently distributed on a nanometer scale so that the ratio of metal and acid sites is rather constant and optimal and the chance of (secondary) cracking becomes smaller.[13,31,32,47,83−86] The hydroconversion of larger hydrocarbons such as n-C_{16} and their mechanism has already been studied significantly. Therefore, in the present study we did not focus on elucidating the hydroconversion mechanism, but we used the n-C_{16} hydroconversion reaction to showcase the influence of nanoscale metal loading heterogeneities on the catalytic performance of a catalyst. Differences in the catalytic performance between uniform and non-uniform distribution of n_{Pt}/n_A over the catalysts were only revealed at relatively low metal loading. For more details on the n-C_{16} hydroconversion mechanism, we refer the reader to literature.[3,5,47,87−89]

It could be argued that the location of Pt inside the zeolite crystal or on the outer surface of the zeolite crystal could have an influence on the catalytic performance as suggested in earlier literature.[57] For impregnated samples, however, it is well known that nearly all metal nanoparticles reside in the zeolite crystals.[52,90] Even if that would not be the case and a significant part of Pt would be on the outer surface of the zeolite crystals, this would have a positive influence on the catalytic performance.[40,91] Additionally, in industry, binders are used to make strong catalyst extrudates and the Pt metal can also be deposited on this binder. In that case, it can be beneficial to have the metal close to the zeolite outer surface, that is the metal on the binder, in order to restrict diffusion limitations of the feedstock and/or the desired products.[6,40,75,92−94] This therefore highlights the fact that not the location of Pt for the CPA-prepared samples but rather the nanoscale heterogeneities were accountable for the decreased catalytic performance, especially when decreasing the metal loading, while a more uniform sample with respect to n_{Pt}/n_A ratio prepared with PTA had a significantly better performance. This is, to the best of our knowledge, the first study that

links nanoscale crystal-based heterogeneities to the performance of bifunctional catalysts for n-alkane hydroconversion.

A summary of the catalytic performance for n-C_7 and n-C_{16} hydroisomerization is given in Figure 6, where the temperature to reach 50% conversion (T_{50}) and the maximum isomer yield (I_{max}) are shown. A decrease of the Pt loading from 1.0 to 0.3 wt % for PTA-prepared samples gave similar results for both n-C_7 and n-C_{16} hydroisomerization. For CPA-prepared samples this decrease of the Pt loading from 1.0 to 0.3 wt % gave rise to similar results in n-C_7 hydroisomerization, but for n-C_{16} hydroisomerization a significant decrease in isomer selectivity was observed. Additionally, this decrease in Pt loading led to a higher amount of secondary cracking during n-C_{16} hydroisomerization for CPA-prepared samples, indicating that non-ideal bifunctional catalysis occurred. Decreasing the metal loading even further to 0.03 wt % Pt led to a decreased catalytic performance in n-C_7 as well as n-C_{16} hydroisomerization, irrespective of the metal precursor.

These results therefore show that there is indeed a minimum amount of Pt sites necessary to obtain ideal bifunctional catalysis, though it should be mentioned that the minimum Pt loading does not appear to be at an n_{Pt}/n_A ratio of 0.17 as reported by Guisnet.[10,16,39] The difference is attributed to varying reaction conditions such as the pressure and the feedstock size.[16,39,42,95,96] The difference between the PTA and CPA series highlights the influence of the nanoscale crystal-based heterogeneities as observed with TEM−EDX measurements, assuming that those heterogeneities also occur at lower Pt loadings. The minimum Pt loading necessary is influenced by such nanoscale metal loading heterogeneities, leading to nanoscale differences in crystal-based n_{Pt}/n_A ratios. While a variety of studies has already paid attention to the intimacy criterion to optimize bifunctional catalysts' performance, this is to the best of our knowledge the first study that correlates the influence of nanoscale metal loading heterogeneities to the catalytic hydroisomerization performance.

■ CONCLUSIONS AND OUTLOOK

The influence of the metal precursor and loading is often addressed in literature, mainly focusing on dispersing metal nanoparticles as optimally as possible. In this research it was shown that for Pt/zeolite Y bifunctional catalysts the metal precursor and loading are important for the impact and control

of metal loading heterogeneities at the nanoscale. In this study, it was demonstrated for the first time that a constant ratio of Pt surface sites and acid sites, n_{Pt}/n_A, per individual zeolite crystal is important for the catalyst performance. In general, many bulk-scale properties between the PTA- and CPA-prepared catalysts were similar, with only differences in the n_{Pt}/n_A ratio from zeolite crystal to zeolite crystal. When the Pt loading was lowered, and thus the bulk n_{Pt}/n_A decreased, nanoscale structures, such as Pt particle size and local n_{Pt}/n_A ratio differences, became more crucial for optimal catalytic performance, which was clearly shown for CPA-prepared samples. It was shown that the Pt loading can be lowered significantly for PTA-prepared samples, while catalytic performance was maintained. Despite the fact that we had to rely on extrapolation to a certain extent, as individual zeolite crystal EDX measurements on those low Pt loadings were not possible due to the detection limit, we believe that with future improvements in imaging systems and EDX detectors, more structural differences in low-loading catalysts can be unraveled, explaining differences in catalytic behavior. By correlating nanoscale parameters to catalytic behavior, more understanding of the influence of the synthesis method and precursor with respect to nanoscale metal loading heterogeneities on the catalytic performance can be gained. This can hopefully lead to optimized catalyst synthesis procedures and to a decrease in noble metal loading necessary for performing catalytic reactions, which is desirable in view of economic and sustainability perspectives.

ASSOCIATED CONTENT

ⓈⒾ Supporting Information

The Supporting Information is available free of charge at https://pubs.acs.org/doi/10.1021/acscatal.1c00211.

> XRD diffractograms, N_2-physisorption isotherms, NH_3-TPD measurements, FT-IR measurements of pyridine, TEM−EDX data, n-C_7 hydroisomerization data, and particle size histograms before and after catalysis, and n-C_{16} isomerization data (PDF)

AUTHOR INFORMATION

Corresponding Author

Krijn P. de Jong − Inorganic Chemistry and Catalysis, Debye Institute for Nanomaterials Science, Utrecht University, 3584 CG Utrecht, The Netherlands; Ⓞ orcid.org/0000-0002-9773-8110; Email: K.P.deJong@uu.nl

Authors

Lars I. van der Wal − Inorganic Chemistry and Catalysis, Debye Institute for Nanomaterials Science, Utrecht University, 3584 CG Utrecht, The Netherlands

Jogchum Oenema − Inorganic Chemistry and Catalysis, Debye Institute for Nanomaterials Science, Utrecht University, 3584 CG Utrecht, The Netherlands

Luc C. J. Smulders − Inorganic Chemistry and Catalysis, Debye Institute for Nanomaterials Science, Utrecht University, 3584 CG Utrecht, The Netherlands

Nonne J. Samplonius − Inorganic Chemistry and Catalysis, Debye Institute for Nanomaterials Science, Utrecht University, 3584 CG Utrecht, The Netherlands

Karan R. Nandpersad − Inorganic Chemistry and Catalysis, Debye Institute for Nanomaterials Science, Utrecht University, 3584 CG Utrecht, The Netherlands

Jovana Zečević − Inorganic Chemistry and Catalysis, Debye Institute for Nanomaterials Science, Utrecht University, 3584 CG Utrecht, The Netherlands

Complete contact information is available at:
https://pubs.acs.org/10.1021/acscatal.1c00211

Author Contributions

The manuscript was written through contributions of all authors. All authors have given approval to the final version of the manuscript.

Notes

The authors declare no competing financial interest.

■ REFERENCES

(1) Arribas, M. A.; Martínez, A. The Influence of Zeolite Acidity for the Coupled Hydrogenation and Ring Opening of 1-Methylnaphthalene on Pt/USY Catalysts. *Appl. Catal., A* **2002**, *230*, 203−217.

(2) Martens, G. G.; Marin, G. B.; Martens, J. A.; Jacobs, P. A.; Baron, G. V. A Fundamental Kinetic Model for Hydrocracking of C_8 to C_{12} Alkanes on Pt/US-Y Zeolites. *J. Catal.* **2000**, *195*, 253−267.

(3) Park, K.-C.; Ihm, S.-K. Comparison of Pt/Zeolite Catalysts for n-Hexadecane Hydroisomerization. *Appl. Catal., A* **2000**, *203*, 201−209.

(4) Patrigeon, A.; Benazzi, E.; Travers, C.; Bernhard, J. Y. Influence of the Zeolite Structure and Acidity on the Hydroisomerization of n-Heptane. *Catal. Today* **2001**, *65*, 149−155.

(5) Weitkamp, J. Catalytic Hydrocracking-Mechanisms and Versatility of the Process. *ChemCatChem* **2012**, *4*, 292−306.

(6) Zecevic, J.; Vanbutsele, G.; de Jong, K. P.; Martens, J. A. Nanoscale Intimacy in Bifunctional Catalysts for Selective Conversion of Hydrocarbons. *Nature* **2015**, *528*, 245−248.

(7) Maxwell, I. E. Zeolite Catalysis in Hydroprocessing Technology. *Catal. Today* **1987**, *1*, 385−413.

(8) Vogt, E. T. C.; Whiting, G. T.; Dutta Chowdhury, A.; Weckhuysen, B. M. Zeolites and Zeotypes for Oil and Gas Conversion. *Adv. Catal.* **2015**, *58*, 143−314.

(9) Peng, B.; Yao, Y.; Zhao, C.; Lercher, J. A. Towards Quantitative Conversion of Microalgae Oil to Diesel-Range Alkanes with Bifunctional Catalysts. *Angew. Chem., Int. Ed.* **2012**, *51*, 2072−2075.

(10) Alvarez, F.; Ribeiro, F. R.; Perot, G.; Thomazeau, C.; Guisnet, M. Hydroisomerization and Hydrocracking of Alkanes. *J. Catal.* **1996**, *162*, 179−189.

(11) de Graaf, J.; van Dillen, A. J.; de Jong, K. P.; Koningsberger, D. C. Preparation of Highly Dispersed Pt Particles in Zeolite Y with a Narrow Particle Size Distribution: Characterization by Hydrogen Chemisorption, TEM, EXAFS Spectroscopy, and Particle Modeling. *J. Catal.* **2001**, *203*, 307−321.

(12) Prieto, G.; Zečević, J.; Friedrich, H.; de Jong, K. P.; de Jongh, P. E. Towards Stable Catalysts by Controlling Collective Properties of Supported Metal Nanoparticles. *Nat. Mater.* **2013**, *12*, 34−39.

(13) Weisz, P. B. Polyfunctional Heterogeneous Catalysis. *Adv. Catal.* **1962**, *13*, 137−190.

(14) Murzin, D. Y. Mesolevel Bifunctional Catalysis. *Kinet. Catal.* **2020**, *61*, 80−92.

(15) Murzin, D. Y. On Spatial Control in Heterogeneous Multifunctional Catalysts. *Catal. Lett.* **2017**, *147*, 613−621.

(16) Guisnet, M.; Alvarez, F.; Giannetto, G.; Perot, G. Hydroisomerization and Hydrocracking of n-Heptane on PtH Zeolites.

Effect of the Porosity and of the Distribution of Metallic and Acid Sites. *Catal. Today* **1987**, *1*, 415−433.

(17) Vermeiren, W.; Gilson, J.-P. Impact of Zeolites on the Petroleum and Petrochemical Industry. *Top. Catal.* **2009**, *52*, 1131−1161.

(18) de Jong, K. P.; Zečević, J.; Friedrich, H.; de Jongh, P. E.; Bulut, M.; van Donk, S.; Kenmogne, R.; Finiels, A.; Hulea, V.; Fajula, F. Zeolite Y Crystals with Trimodal Porosity as Ideal Hydrocracking Catalysts. *Angew. Chem., Int. Ed.* **2010**, *49*, 10074−10078.

(19) Deldari, H. Suitable Catalysts for Hydroisomerization of Long-Chain Normal Paraffins. *Appl. Catal., A* **2005**, *293*, 1−10.

(20) Pérez-Ramírez, J.; Christensen, C. H.; Egeblad, K.; Christensen, C. H.; Groen, J. C. Hierarchical Zeolites: Enhanced Utilisation of Microporous Crystals in Catalysis by Advances in Materials Design. *Chem. Soc. Rev.* **2008**, *37*, 2530−2542.

(21) Li, K.; Valla, J.; Garcia-Martinez, J. Realizing the Commercial Potential of Hierarchical Zeolites: New Opportunities in Catalytic Cracking. *ChemCatChem* **2014**, *6*, 46−66.

(22) van Donk, S.; Janssen, A. H.; Bitter, J. H.; de Jong, K. P. Generation, Characterization, and Impact of Mesopores in Zeolite Catalysts. *Catal. Rev.-Sci. Eng.* **2003**, *45*, 297−319.

(23) Janssen, A. H.; Koster, A. J.; de Jong, K. P. Three-Dimensional Transmission Electron Microscopic Observations of Mesopores in Dealuminated Zeolite Y. *Angew. Chem., Int. Ed.* **2001**, *113*, 1136−1138.

(24) Verboekend, D.; Nuttens, N.; Locus, R.; Van Aelst, J.; Verolme, P.; Perez-Ramirez, J.; Sels, B. F. Synthesis, Characterisation, and Catalytic Evaluation of Hierarchical Faujasite Zeolites: Milestones, Challenges, and Future Directions. *Chem. Soc. Rev.* **2016**, *45*, 3331−3352.

(25) Tao, Y.; Kanoh, H.; Abrams, L.; Kaneko, K. Mesopore-Modified Zeolites: Preparation, Characterization, and Applications. *Chem. Rev.* **2006**, *106*, 896−910.

(26) Groen, J. C.; Moulijn, J. A.; Pérez-Ramírez, J. Desilication: On the Controlled Generation of Mesoporosity in MFI Zeolites. *J. Mater. Chem.* **2006**, *16*, 2121−2131.

(27) Groen, J. C.; Zhu, W.; Brouwer, S.; Huynink, S. J.; Kapteijn, F.; Moulijn, J. A.; Pérez-Ramírez, J. Direct Demonstration of Enhanced Diffusion in Mesoporous ZSM-5 Zeolite Obtained via Controlled Desilication. *J. Am. Chem. Soc.* **2007**, *129*, 355−360.

(28) Park, D. H.; Kim, S. S.; Wang, H.; Pinnavaia, T. J.; Papapetrou, M. C.; Lappas, A. A.; Triantafyllidis, K. S. Selective Petroleum Refining over a Zeolite Catalyst with Small Intracrystal Mesopores. *Angew. Chem., Int. Ed.* **2009**, *48*, 7645−7648.

(29) Egeblad, K.; Christensen, C. H.; Kustova, M.; Christensen, C. H. Templating Mesoporous Zeolites. *Chem. Mater.* **2008**, *20*, 946−960.

(30) Kinger, G.; Vinek, H. n-Nonane Hydroconversion on Ni and Pt Containing HMFI, HMOR and HBEA. *Appl. Catal., A* **2001**, *218*, 139−149.

(31) Lugstein, A.; Jentys, A.; Vinek, H. Hydroconversion of n-Heptane over Bifunctional HZSM5 Zeolites Influence of the Metal Concentration and Distribution on the Activity and Selectivity. *Appl. Catal., A* **1998**, *166*, 29−38.

(32) Blomsma, E.; Martens, J. A.; Jacobs, P. A. Isomerization and Hydrocracking of Heptane over Bimetallic Bifunctional PtPd/H-Beta and PtPd/USY Zeolite Catalysts. *J. Catal.* **1997**, *165*, 241−248.

(33) Ward, J. W. Hydrocracking Processes and Catalysts. *Fuel Process. Technol.* **1993**, *35*, 55−85.

(34) Lemberton, J. L.; Touzeyidio, M.; Guisnet, M. Catalytic Hydroprocessing of Simulated Coal Tars. I. Activity of a Sulphided Ni-Mo/Al$_2$O$_3$ Catalyst for the Hydroconversion of Model Compounds. *Appl. Catal.* **1989**, *54*, 91−100.

(35) Lemberton, J. L.; Touzeyidio, M.; Guisnet, M. Catalytic Hydroprocessing of Simulated Coal Tars. II. Effect of Acid Catalysts on the Hydroconversion of Model Compounds on a Sulphided Ni-Mo/Al$_2$O$_3$ Catalyst. *Appl. Catal.* **1989**, *54*, 101−109.

(36) Sato, K.; Iwata, Y.; Miki, Y.; Shimada, H. Hydrocracking of Tetralin over NiW/USY Zeolite Catalysts: For the Improvement of Heavy-Oil Upgrading Catalysts. *J. Catal.* **1999**, *186*, 45−56.

(37) Lee, S.-W.; Ihm, S.-K. Hydroisomerization and Hydrocracking over Platinum Loaded ZSM-23 Catalysts in the Presence of Sulfur and Nitrogen Compounds for the Dewaxing of Diesel Fuel. *Fuel* **2014**, *134*, 237−243.

(38) Bouchy, C.; Hastoy, G.; Guillon, E.; Martens, J. A. Fischer-Tropsch Waxes UpgradingviaHydrocracking and Selective Hydroisomerization. *Oil Gas Sci. Technol.* **2009**, *64*, 91−112.

(39) Guisnet, M. "Ideal" bifunctional catalysis over Pt-acid zeolites. *Catal. Today* **2013**, *218−219*, 123−134.

(40) Wang, W.; Liu, C.-J.; Wu, W. Bifunctional catalysts for the hydroisomerization of n-alkanes: the effects of metal-acid balance and textural structure. *Catal. Sci. Technol.* **2019**, *9*, 4162−4187.

(41) Zhang, W.; Smirniotis, P. G. Effect of Zeolite Structure and Acidity on the Product Selectivity and Reaction Mechanism for n-Octane Hydroisomerization and Hydrocracking. *J. Catal.* **1999**, *182*, 400−416.

(42) Thybaut, J. W.; Laxmi Narasimhan, C. S.; Denayer, J. F.; Baron, G. V.; Jacobs, P. A.; Martens, J. A.; Marin, G. B. Acid-Metal Balance of a Hydrocracking Catalyst: Ideal versus Nonideal Behavior. *Ind. Eng. Chem. Res.* **2005**, *44*, 5159−5169.

(43) Merabti, R.; Pinard, L.; Lemberton, J. L.; Magnoux, P.; Barama, A.; Moljord, K. Effect of Na Exchange of a HBEA Zeolite on the Activity and the Selectivity of a Bifunctional Pt-HBEA Catalyst for n-Hexadecane Hydroisomerization. Comparison with a Pt-HZSM-22 Catalyst. *React. Kinet., Mech. Catal.* **2010**, *100*, 1−9.

(44) Benazzi, E.; Leite, L.; Marchal-George, N.; Toulhoat, H.; Raybaud, P. New Insights into Parameters Controlling the Selectivity in Hydrocracking Reactions. *J. Catal.* **2003**, *217*, 376−387.

(45) Galperin, L. B.; Bradley, S. A.; Mezza, T. M. Hydro-isomerization of n-Decane in the Presence of Sulfur: Effect of Metal-Acid Balance and Metal Location. *Appl. Catal., A* **2001**, *219*, 79−88.

(46) Batalha, N.; Pinard, L.; Pouilloux, Y.; Guisnet, M. Bifunctional Hydrogenating/Acid Catalysis: Quantification of the Intimacy Criterion. *Catal. Lett.* **2013**, *143*, 587−591.

(47) Batalha, N.; Pinard, L.; Bouchy, C.; Guillon, E.; Guisnet, M. n-Hexadecane Hydroisomerization over Pt-HBEA Catalysts. Quantification and Effect of the Intimacy between Metal and Protonic Sites. *J. Catal.* **2013**, *307*, 122−131.

(48) Roldán, R.; Romero, F. J.; Jiménez-Sanchidrián, C.; Marinas, J. M.; Gómez, J. P. Influence of Acidity and Pore Geometry on the Product Distribution in the Hydroisomerization of Light Paraffins on Zeolites. *Appl. Catal., A* **2005**, *288*, 104−115.

(49) Munnik, P.; De Jongh, P. E.; de Jong, K. P. Recent Developments in the Synthesis of Supported Catalysts. *Chem. Rev.* **2015**, *115*, 6687−6718.

(50) Plessers, E.; Stassen, I.; Sree, S. P.; Janssen, K. P. F.; Yuan, H.; Martens, J.; Hofkens, J.; de Vos, D.; Roeffaers, M. B. J. Resolving Interparticle Heterogeneities in Composition and Hydrogenation Performance between Individual Supported Silver on Silica Catalysts. *ACS Catal.* **2015**, *5*, 6690−6695.

(51) Plessers, E.; van den Reijen, J. E.; de Jongh, P. E.; de Jong, K. P.; Roeffaers, M. B. J. Origin and Abatement of Heterogeneity at the Support Granule Scale of Silver on Silica Catalysts. *ChemCatChem* **2017**, *9*, 4562−4569.

(52) Zečević, J.; van der Eerden, A. M. J.; Friedrich, H.; de Jongh, P. E.; de Jong, K. P. Heterogeneities of the Nanostructure of Platinum/Zeolite Y Catalysts Revealed by Electron Tomography. *ACS Nano* **2013**, *7*, 3698−3705.

(53) van der Wal, L. I.; de Jong, K. P.; Zečević, J. The Origin of Metal Loading Heterogeneities in Pt/Zeolite Y Bifunctional Catalysts. *ChemCatChem* **2019**, *11*, 4081−4088.

(54) Wang, Y.; Tao, Z.; Wu, B.; Xu, J.; Huo, C.; Li, K.; Chen, H.; Yang, Y.; Li, Y. Effect of metal precursors on the performance of Pt/ZSM-22 catalysts for n-hexadecane hydroisomerization. *J. Catal.* **2015**, *322*, 1−13.

(55) Torres, H. M.; Koeken, A. C. J.; Bitter, J. H.; Davidian, T.; Ruitenbeek, M.; Dugulan, A. I.; de Jong, K. P. Effect of Precursor on the Catalytic Performance of Supported Iron Catalysts for the Fischer–Tropsch Synthesis of Lower Olefins. *Catal. Today* **2013**, *215*, 95–102.

(56) Geng, L.; Gong, J.; Qiao, G.; Ye, S.; Zheng, J.; Zhang, N.; Chen, B. Effect of Metal Precursors on the Performance of Pt/SAPO-11 Catalysts for n-Dodecane Hydroisomerization. *ACS Omega* **2019**, *4*, 12598–12605.

(57) Tsai, K.-Y.; Wang, I.; Tsai, T.-C. Zeolite Supported Platinum Catalysts for Benzene Hydrogenation and Naphthene Isomerization. *Catal. Today* **2011**, *166*, 73–78.

(58) Gopal, S.; Smirniotis, P. G. Factors Affecting Isomer Yield for n-Heptane Hydroisomerization over as-Synthesized and Dealuminated Zeolite Catalysts Loaded with Platinum. *J. Catal.* **2004**, *225*, 278–287.

(59) Emeis, C. A. Determination of Integrated Molar Extinction Coefficients for Infrared Absorption Bands of Pyridine Adsorbed on Solid Acid Catalysts. *J. Catal.* **1993**, *141*, 347–354.

(60) Busca, G. Spectroscopic Characterization of the Acid Properties of Metal Oxide Catalysts. *Catal. Today* **1998**, *41*, 191–206.

(61) Velthoen, M. E. Z.; Nab, S.; Weckhuysen, B. M. Probing Acid Sites in Solid Catalysts with Pyridine UV-Vis Spectroscopy. *Phys. Chem. Chem. Phys.* **2018**, *20*, 21647–21659.

(62) Oudenhuijzen, M. K.; Kooyman, P. J.; Tappel, B.; Van Bokhoven, J. A.; Koningsberger, D. C. Understanding the Influence of the Pretreatment Procedure on Platinum Particle Size and Particle-Size Distribution for SiO$_2$ Impregnated with $[Pt^{2+}(NH_3)_4](NO_3^-)_2$: A Combination of HRTEM, Mass Spectrometry, and Quick EXAFS. *J. Catal.* **2002**, *205*, 135–146.

(63) Van Den Broek, A. C. M.; Van Grondelle, J.; Van Santen, R. A. Preparation of Highly Dispersed Platinum Particles in HZSM-5 Zeolite: A Study of the Pretreatment Process of $[Pt(NH_3)_4]^{2+}$. *J. Catal.* **1997**, *167*, 417–424.

(64) Malet, P.; Munuera, G.; Caballero, A. Effect of Chlorine in the Formation of PtRe Alloys in PtRe Al$_2$O$_3$ Catalysts. *J. Catal.* **1989**, *115*, 567–579.

(65) Lieske, H.; Lietz, G.; Spindler, H.; Völter, J. Reactions of platinum in oxygen- and hydrogen-treated Pt/γ-Al$_2$O$_3$ catalysts I. Temperature-programmed reduction, adsorption, and redispersion of platinum. *J. Catal.* **1983**, *81*, 8–16.

(66) Borgna, A.; Garetto, T. F.; Apesteguía, C. R.; Le Normand, F.; Moraweck, B. Sintering of Chlorinated Pt/γ-Al$_2$O$_3$ Catalysts: An In Situ Study by X-Ray Absorption Spectroscopy. *J. Catal.* **1999**, *186*, 433–441.

(67) da Silva, M. A. P.; Mellovieira, R. A.; Schmal, M. Interaction between Pt and MoO$_3$ Dispersed over Alumina. *Appl. Catal., A* **2000**, *190*, 177–190.

(68) Remy, M. J.; Stanica, D.; Poncelet, G.; Feijen, E. J. P.; Grobet, P. J.; Martens, J. A.; Jacobs, P. A.; Dealuminated, H.-Y. Dealuminated H-Y Zeolites: Relation between Physicochemical Properties and Catalytic Activity in Heptane and Decane Isomerization. *J. Phys. Chem.* **1996**, *100*, 12440–12447.

(69) Boréave, A.; Auroux, A.; Guimon, C. Nature and Strength of Acid Sites in HY Zeolites: A Multitechnical Approach. *Microporous Mater.* **1997**, *11*, 275–291.

(70) Andreev, A. S.; Livadaris, V. Characterization of Catalytic Materials through a Facile Approach to Probe OH Groups by Solid-State NMR. *J. Phys. Chem. C* **2017**, *121*, 14108–14119.

(71) Hadjiivanov, K. Identification and Characterization of Surface Hydroxyl Groups by Infrared Spectroscopy. *Adv. Catal.* **2014**, *57*, 99–318.

(72) Weisz, P. B.; Prater, C. D. Interpretation of Measurements in Experimental Catalysis. *Adv. Catal.* **1954**, *6*, 143–196.

(73) Bischoff, K. B. An Extension of the General Criterion for Importance of Pore Diffusion with Chemical Reactions. *Chem. Eng. Sci.* **1967**, *22*, 525–530.

(74) Moulijn, J. A.; Makkee, M.; Berger, R. J. Catalyst Testing in Multiphase Micro-Packed-Bed Reactors; Criterion for Radial Mass Transport. *Catal. Today* **2016**, *259*, 354–359.

(75) Cheng, K.; van der Wal, L. I.; Yoshida, H.; Oenema, J.; Harmel, J.; Zhang, Z.; Sunley, G.; Zečević, J.; de Jong, K. P. Impact of the Spatial Organization of Bifunctional Metal-Zeolite Catalysts on the Hydroisomerization of Light Alkanes. *Angew. Chem., Int. Ed.* **2020**, *59*, 3592–3600.

(76) Vu, T.; Van Gestel, J.; Gilson, J.; Collet, C.; Dath, J.; Duchet, J. Platinum-tungstated Zirconia Isomerization Catalysts Part II. Effect of Platinum and Tungsten Loading on the Mechanism of Isomerization of n-Hexane: a Kinetic Study. *J. Catal.* **2005**, *231*, 468–479.

(77) Blomsma, E.; Martens, J. A.; Jacobs, P. A. Reaction Mechanisms of Heptane Isomerization and Cracking on Bifunctional Pt/H-Beta Zeolites. *Stud. Surf. Sci. Catal.* **1997**, *105*, 909–916.

(78) Blomsma, E.; Martens, J. A.; Jacobs, P. A. Reaction Mechanisms of Isomerization and Cracking of Heptane on Pd/H-Beta Zeolite. *J. Catal.* **1995**, *155*, 141–147.

(79) Blomsma, E.; Martens, J. A.; Jacobs, P. A. Mechanisms of Heptane Isomerization on Bifunctional Pd/H-Beta Zeolites. *J. Catal.* **1996**, *159*, 323–331.

(80) McClellan, A. L.; Harnsberger, H. F. Cross-Sectional Areas of Molecules Adsorbed on Solid Surfaces. *J. Colloid Interface Sci.* **1967**, *23*, 577–599.

(81) Gray, M. J.; Mebane, R. C.; Womack, H. N.; Rybolt, T. R. Molecular Mechanics and Molecular Cross-Sectional Areas: A Comparison with Molecules Adsorbed on Solid Surfaces. *J. Colloid Interface Sci.* **1995**, *170*, 98–101.

(82) Liu, F. P.; Rials, T. G.; Simonsen, J. Relationship of Wood Surface Energy to Surface Composition. *Langmuir* **1998**, *14*, 536–541.

(83) Zhang, A.; Nakamura, I.; Aimoto, K.; Fujimoto, K. Isomerization of n-Pentane and Other Light Hydrocarbons on Hybrid Catalyst. Effect of Hydrogen Spillover. *Ind. Eng. Chem. Res.* **1995**, *34*, 1074–1080.

(84) Ali, M. A.; Tatsumi, T.; Masuda, T. Development of Heavy Oil Hydrocracking Catalysts Using Amorphous Silica-Alumina and Zeolites as Catalyst Supports. *Appl. Catal., A* **2002**, *233*, 77–90.

(85) Cui, Q.; Zhou, Y.; Wei, Q.; Tao, X.; Yu, G.; Wang, Y.; Yang, J. Role of the Zeolite Crystallite Size on Hydrocracking of Vacuum Gas Oil over NiW/Y-ASA Catalysts. *Energy Fuels* **2012**, *26*, 4664–4670.

(86) Chen, H.; Yi, F.; Ma, C.; Gao, X.; Liu, S.; Tao, Z.; Wu, B.; Xiang, H.; Yang, Y.; Li, Y.-w. Hydroisomerization of n-Heptane on a New Kind of Bifunctional Catalysts with Palladium Nanoparticles Encapsulating inside Zeolites. *Fuel* **2020**, *268*, 117241.

(87) Mendes, P. S. F.; Silva, J. M.; Ribeiro, M. F.; Daudin, A.; Bouchy, C. Bifunctional Intimacy and its Interplay with Metal-Acid Balance in Shaped Hydroisomerization Catalysts. *ChemCatChem* **2020**, *12*, 4582–4592.

(88) Soualah, A.; Lemberton, J. L.; Pinard, L.; Chater, M.; Magnoux, P.; Moljord, K. Hydroisomerization of Long-Chain n-Alkanes on Bifunctional Pt/Zeolite Catalysts: Effect of the Zeolite Structure on the Product Selectivity and on the Reaction Mechanism. *Appl. Catal., A* **2008**, *336*, 23–28.

(89) Kumar, H.; Froment, G. F. A Generalized Mechanistic Kinetic Model for the Hydroisomerization and Hydrocracking of Long-Chain Paraffins. *Ind. Eng. Chem. Res.* **2007**, *46*, 4075–4090.

(90) Zečević, J.; van der Eerden, A. M. J.; Friedrich, H.; de Jongh, P. E.; de Jong, K. P. H$_2$PtCl$_6$-Derived Pt Nanoparticles on USY Zeolite: A Qualitative and Quantitative Electron Tomography Study. *Microporous Mesoporous Mater.* **2012**, *164*, 99–103.

(91) Kim, J.; Kim, W.; Seo, Y.; Kim, J.-C.; Ryoo, R. n-Heptane Hydroisomerization over Pt/MFI Zeolite Nanosheets: Effects of Zeolite Crystal Thickness and Platinum Location. *J. Catal.* **2013**, *301*, 187–197.

(92) Oenema, J.; Harmel, J.; Vélez, R. P.; Meijerink, M. J.; Eijsvogel, W.; Poursaeidesfahani, A.; Vlugt, T. J. H.; Zečević, J.; De Jong, K. P. Influence of Nanoscale Intimacy and Zeolite Micropore Size on the

Performance of Bifunctional Catalysts for n-Heptane Hydroisomerization. *ACS Catal.* **2020**, *10*, 14245−14257.

(93) Camblor, M. A.; Corma, A.; Martínez, A.; Martínez-Soria, V.; Valencia, S. Mild Hydrocracking of Vacuum Gasoil over NiMo-Beta Zeolite Catalysts: The Role of the Location of the NiMo Phases and the Crystallite Size of the Zeolite. *J. Catal.* **1998**, *179*, 537−547.

(94) Ben Moussa, O.; Tinat, L.; Jin, X.; Baaziz, W.; Durupthy, O.; Sayag, C.; Blanchard, J. Heteroaggregation and Selective Deposition for the Fine Design of Nanoarchitectured Bifunctional Catalysts: Application to Hydroisomerization. *ACS Catal.* **2018**, *8*, 6071−6078.

(95) Grau, J. M.; Parera, J. M. Conversion of Heavy n-Alkanes into Light Isomers over H-Mordenite, Platinum/H-Mordenite, Platinum/Alumina and Composite Catalysts. *Appl. Catal., A* **1993**, *106*, 27−49.

(96) Mendes, P. S. F.; Chizallet, C.; Pérez-Pellitero, J.; Raybaud, P.; Silva, J. M.; Ribeiro, M. F.; Daudin, A.; Bouchy, C. Interplay of the Adsorption of Light and Heavy Paraffins in Hydroisomerization over H-Beta Zeolite. *Catal. Sci. Technol.* **2019**, *9*, 5368−5382.